LAMINATE DESIGN FOR IMPROVED POST-CRITICALLY STABLE PERFORMANCE

C. B. York[1]

[1] Singapore Institute of Technology, 10 Dover Drive, Singapore 138683
Christopher.York@singaporetech.edu.sg
www.singaporetech.edu.sg/directory/faculty/christopher-bronn-york

Keywords: Double angle-ply laminates, Standard ply laminates, Post-buckling, Stiffness matching.

ABSTRACT

This article discusses laminate performance, relating to pre- and post-critically stable in-plane response, for double angle-ply laminates (with $\pm\psi$ and $\pm\phi$ ply orientations), which are stiffness matched to equivalent standard symmetric laminate configurations; all with fully uncoupled stiffness properties or *Extension-Shearing* coupling. Results are normalised against the fully isotropic laminate response in order to highlight laminate configurations that maximise post critical in-plane stiffness.

1 INTRODUCTION

Double angle-ply laminates have been shown to offer greater potential for stiffness tailoring and improvements in strength [1], together with ease of manufacturability [2], when compared to standard ply laminates. However, little consideration has been given to performance indicators relating to bending stiffness. This has been addressed only recently for initial buckling performance [3]. However, post-buckling performance is influenced by extensional stiffness as well as bending stiffness, since the post critical load carrying capacity depends on how the membrane stresses are redistributed. Also considered here is the post-buckling response of off-axis aligned laminate designs, which maximise *Extension-Shearing* coupling. Such design have been shown [4] to provide the necessary coupling for drag reduction in aero-elastically tailored wing skins.

3 METHODOLOGY

A new database of double angle-ply laminate configurations, containing specific mechanical coupling characteristics, is used in conjunction with a stiffness matching approach [3] to obtain tailored laminate designs with identical bending or extensional stiffness. This permits performance comparisons with standard symmetric laminate configurations, to which design heuristics are also applied, i.e., limiting the proportion of plies in each of the standard fibre directions (0, ±45, 90°) to a minimum of 10% as well as a maximum of 3 adjacent plies with the same orientation.

3.1 Database of standard symmetric laminate configurations

A database of design information for fully uncoupled symmetric laminates with up to 21 plies [5] is summarized Fig. 1 and Table 1; all are within the 10% rule design space and with a ply contiguity constraint of no more than 3 adjacent plies with identical orientation. Examples of the unique lamination parameter design points of Fig. 1(a) are presented in Table 1, however, only points within one symmetric half of the design space ($\xi_1 \geq 0$) are listed. The other designs may be obtained by switching 0 and 90° plies in the stacking sequences. The examples given were chosen because they represent solutions with the highest buckling factor above the isotropic asymptote ($k_x/k_{x\text{-}Iso}$).

Ply percentage mapping for standard ply laminates are superimposed on the lamination parameter design space illustrated in Fig. 1, where the in-plane lamination parameters (ξ_1, ξ_2) for typical aircraft components are also given: Spar (0, -0.6), Skin (0.32, 0.12) and Stiffener (0.5, 0.4). These correspond, respectively, to the following ply percentages for 0°, ±45° and 90° ply orientations: Spar (10/80/10), Skin (44/44/12) and Stiffener (60/30/10). Tables A1and A2 list the symmetric laminates most closely matching typical Skin and Spar panel properties.

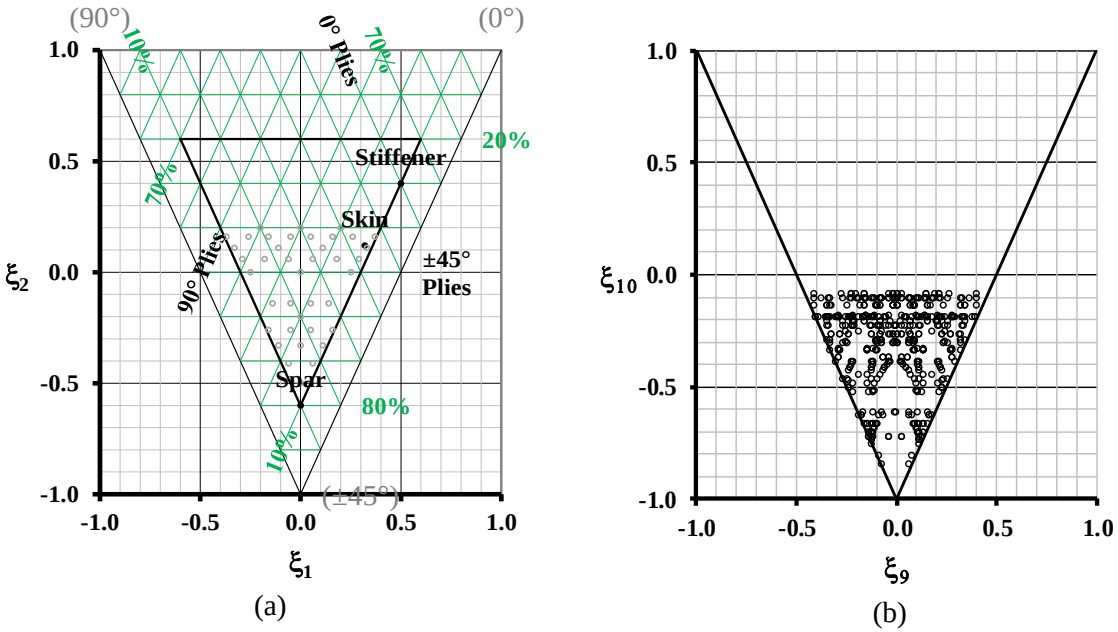

Figure 1: Lamination parameter design spaces for fully uncoupled symmetric laminates ($12 \leq n \leq 21$ plies), representing: (a) 39 unique design points in extensional stiffness and (b) the corresponding points in bending stiffness.

n	Stacking Sequence	ξ_1	ξ_2	ξ_9	ξ_{10}	$k_x/k_{x\text{-Iso}}$
19	$[45/0/-45/-45/0/0/0/45/90/\underline{0}]_S$	0.37	0.16	0.40	-0.19	4.7%
18	$[45/0/-45/-45/0/0/0/90/45]_S$	0.33	0.11	0.38	-0.20	4.8%
17	$[45/-45/0/0/-45/0/90/45/\underline{0}]_S$	0.29	0.06	0.32	-0.27	6.7%
19	$[45/0/-45/-45/0/0/0/45/90/\underline{90}]_S$	0.26	0.16	0.40	-0.19	4.7%
16	$[45/-45/0/-45/0/45/90/0]_S$	0.25	0.00	0.24	-0.47	11.5%
20	$[45/-45/0/0/-45/0/45/90/0/90]_S$	0.20	0.20	0.34	-0.23	5.7%
19	$[45/0/-45/-45/0/0/90/45/90/\underline{0}]_S$	0.16	0.16	0.33	-0.19	4.7%
19	$[45/-45/-45/0/45/45/-45/0/90/\underline{0}]_S$	0.16	-0.26	0.14	-0.71	17.4%
21	$[45/-45/-45/0/45/45/-45/0/0/90/\underline{90}]_S$	*0.14*	*-0.14*	0.16	-0.67	16.5%
14	$[45/-45/0/-45/90/0/45]_S$	*0.14*	*-0.14*	0.14	-0.49	12.1%
18	$[45/0/-45/-45/0/0/90/90/45]_S$	0.11	0.11	0.33	-0.20	4.8%
18	$[45/-45/-45/0/45/45/-45/0/90]_S$	0.11	-0.33	0.13	-0.73	17.9%
17	$[45/-45/-45/0/45/45/-45/90/\underline{0}]_S$	0.06	-0.41	0.12	-0.74	18.2%
17	$[45/-45/0/0/-45/90/90/45/\underline{0}]_S$	0.06	0.06	0.23	-0.27	6.7%
19	$[45/0/-45/-45/0/0/90/45/90/\underline{90}]_S$	0.05	0.16	0.33	-0.19	4.7%
19	$[45/-45/-45/0/45/45/-45/0/90/90]_S$	0.05	-0.26	0.14	-0.71	17.4%
21	$[45/-45/-45/0/45/45/-45/0/90/90/\underline{0}]_S$	0.05	-0.14	0.14	-0.67	16.5%
12	$[45/-45/-45/90/45/0]_S$	0.00	-0.33	-0.08	-0.81	20.0%
16	$[45/-45/-45/45/0/-45/45/90]_S$	0.00	-0.50	0.07	-0.85	20.9%
20	$[45/-45/0/0/-45/90/45/90/0/90]_S$	0.00	0.20	0.22	-0.23	5.7%
16	$[45/-45/0/-45/90/45/90/0]_S$	0.00	0.00	0.09	-0.47	11.5%
20	$[45/-45/-45/0/45/45/-45/90/0/90]_S$	0.00	-0.20	0.11	-0.69	17.0%

Table 1 – Example stacking sequences (mid-plane plies denoted by an underscore) representing fully uncoupled symmetric laminates with optimum buckling strength for a square plate configuration.

For laminates with up to 21 plies, all 39 points in the design space are unique to a single ply number grouping (n), with the exception of the 14- and 21-ply laminates, which shares a common lamination parameter point. This results in 41 distinct groups of fully uncoupled laminates, each with matching extensional stiffness. They represent a total of 527 designs, of which 507 are unique designs, and fall within ply number groupings n = 12, 14, 16 – 21 plies. There are 566 unique designs if the contiguity factor constraint is relaxed. A typical Stiffener component, with coordinate, (ξ_1, ξ_2) = (0.5, 0.4) on Fig. 1, therefore requires a symmetric design with either a higher ply number grouping n > 21, ply contiguity > 3 or a *Bending-Twisting* coupled design. The additional constraint of an outer surface angle-ply is also imposed in all the designs investigated, for the purposes of improved damage tolerance, as is common design practice.

3.2 Database of double angle-ply laminate configurations

The lamination parameter design space of variable double angle-ply laminates [3] differs considerably from that for standard ply designs. Figure 1 represents the lamination parameter design space in extensional stiffness for the fully uncoupled 16-ply double angle-ply laminates of Table 2, all of which have anti-symmetric stacking sequences.

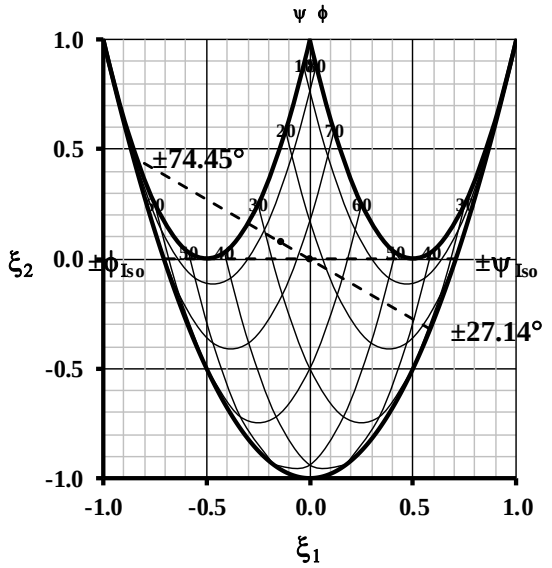

Figure 2: Lamination parameter design spaces for extensional stiffness for laminates *a* - *f* of Table 2.

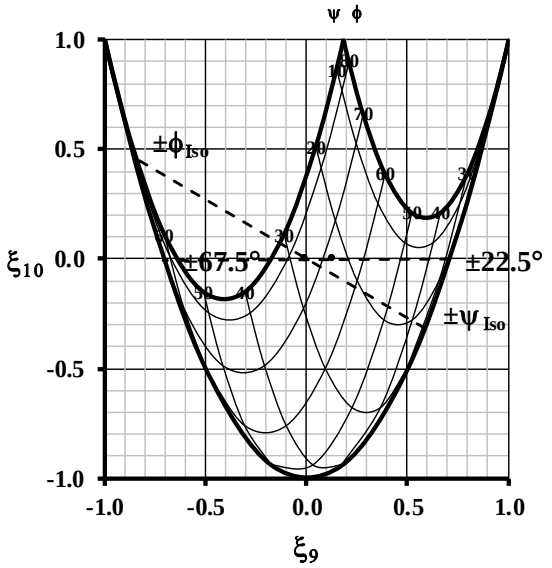

Figure 3: Lamination parameter design space for bending stiffness, representing laminates *c* and *f* of Table 2.

Ref.	Stacking sequence	($\zeta_{\pm\phi}/\zeta$)	($\zeta_{\pm\psi}/\zeta$)	ϕ_{Iso}	ψ_{Iso}
a, b	$[\underline{\psi}/\underline{-\psi}/\underline{-\psi}/\underline{\psi}/\underline{-\phi}/\underline{\phi}/\underline{\phi}/\underline{-\phi}]_A$, $[\underline{\psi}/\underline{-\psi}/\underline{-\psi}/\underline{\psi}/\underline{\phi}/\underline{-\phi}/\underline{-\phi}/\underline{\phi}]_A$	0.12	0.88	-	-
c, f	$[\underline{\psi}/\underline{-\psi}/\underline{\phi}/\underline{-\phi}/\underline{-\phi}/\underline{\phi}/\underline{-\psi}/\underline{\psi}]_A$, $[\underline{\psi}/\underline{-\psi}/\underline{-\phi}/\underline{\phi}/\underline{\phi}/\underline{-\phi}/\underline{-\psi}/\underline{\psi}]_A$	0.40	0.60	74.45°	27.14°
d, e	$[\underline{\psi}/\underline{-\psi}/\underline{\phi}/\underline{-\phi}/\underline{-\psi}/\underline{\psi}/\underline{-\phi}/\underline{\phi}]_A$, $[\underline{\psi}/\underline{-\psi}/\underline{-\phi}/\underline{\phi}/\underline{-\psi}/\underline{\psi}/\underline{\phi}/\underline{-\phi}]_A$	0.31	0.69	-	-

Table 2: Stacking sequences for fully uncoupled double angle-ply laminates with 16 layers. Bending stiffness proportions ($\zeta_{\pm\phi}/\zeta$) and ($\zeta_{\pm\psi}/\zeta$) are given together with angles (ϕ_{Iso}, ψ_{Iso}) for designs which can provide bending isotropy. Ply proportions ($n_{\pm\phi}/n$) = ($n_{\pm\psi}/n$) = 0.5 for all designs and give extensional isotropy for (ϕ_{Iso}, ψ_{Iso}) = (67.5°, 22.5°).

One of the two design solutions illustrated on Fig. 2 has an angle-ply combination ($\pm\phi$, $\pm\psi$) = ($\pm\phi_{Iso}$, $\pm\psi_{Iso}$) = (±74.45°, ±27.14°), which is represented as two points on the parabolic bounds of the design space, between which a broken line provides a Lever rule representation passing through the

lamination parameter coordinate for extensional stiffness, (ξ_1, ξ_2) = (-0.14, 0.07). The location of this point depends on the relative proportion of each ply angle pair within the laminate.

Isolines, representing constant ply angles ($\pm\phi$, $\pm\psi$) across the design space, reveal the lamination parameter coordinate for any unique ply angle combinations.

A second solution illustrated on Fig. 2, representing ($\pm\phi$, $\pm\psi$) = (67.5°, 22.5°), produces extensional isotropy, corresponding to lamination parameter coordinates (ξ_1, ξ_2) = (0.00, 0.00).

Figure 3 represents the lamination parameter design space for bending stiffness, corresponding to laminates *c* and *f* of Table 2. The coordinates for the solution with ($\pm\phi_{Iso}$, $\pm\psi_{Iso}$) = (±74.45°, ±27.14°) can be seen to match the isotropic laminate in bending, i.e., (ξ_9, ξ_{10}) = (0, 0), and the broken line Lever rule representation now depends on the relative proportion that each angle ply contributes to the overall bending stiffness, ($\zeta_{\pm\phi}/\zeta$) and ($\zeta_{\pm\psi}/\zeta$). A second solution on Fig. 3, representing ($\pm\phi$, $\pm\psi$) = (67.5°, 22.5°), corresponds to the lamination parameter coordinate (ξ_9, ξ_{10}) = (0.13, 0.00), and for which the buckling load factor (k_x = 4.00) for aspect ratio a/b = 1, 2, etc., can easily be verified by a closed form solution [6]. This solution produces orthotropic extensional stiffness properties corresponding to the point (ξ_1, ξ_2) = (-0.14, 0.07) on Fig. 2.

The extensional and bending stiffnesses are readily calculated from the lamination parameter coordinates from Fig. 2 and Fig. 3, respectively, by the following equations with laminate thickness *H*:

$$
\begin{aligned}
A_{11} &= \{U_1 + \xi_1 U_2 + \xi_2 U_3\} \times H & D_{11} &= \{U_1 + \xi_9 U_2 + \xi_{10} U_3\} \times H^3/12 \\
A_{12} = A_{21} &= \{-\xi_2 U_3 + U_4\} \times H & D_{12} = D_{21} &= \{-\xi_{10} U_3 + U_4\} \times H^3/12 \\
A_{16} = A_{61} &= \{\xi_3 U_2/2 + \xi_4 U_3\} \times H & D_{16} = D_{61} &= \{\xi_{11} U_2/2 + \xi_{12} U_3\} \times H^3/12 \\
A_{22} &= \{U_1 - \xi_1 U_2 + \xi_2 U_3\} \times H & D_{22} &= \{U_1 - \xi_9 U_2 + \xi_{10} U_3\} \times H^3/12 \\
A_{26} = A_{62} &= \{\xi_3 U_2/2 - \xi_4 U_3\} \times H & D_{26} = D_{62} &= \{\xi_{11} U_2/2 - \xi_{12} U_3\} \times H^3/12 \\
A_{66} &= \{-\xi_2 U_3 + U_5\} \times H & D_{66} &= \{-\xi_{10} U_3 + U_5\} \times H^3/12
\end{aligned}
\tag{1}
$$

where the laminate invariants are calculated from the reduced stiffness terms, Q_{ij}, and the reduced stiffness terms are calculated from the material properties:

$$
\begin{aligned}
U_1 &= \{3Q_{11} + 3Q_{22} + 2Q_{12} + 4Q_{66}\}/8 & Q_{11} &= E_1/(1 - \nu_{12}\nu_{21}) \\
U_2 &= \{Q_{11} - Q_{22}\}/2 & Q_{12} &= \nu_{12}E_2/(1 - \nu_{12}\nu_{21}) \\
U_3 &= \{Q_{11} + Q_{22} - 2Q_{12} - 4Q_{66}\}/8 & Q_{22} &= E_2/(1 - \nu_{12}\nu_{21}) \\
U_4 &= \{Q_{11} + Q_{22} + 6Q_{12} - 4Q_{66}\}/8 & Q_{66} &= G_{12} \\
U_5 &= \{Q_{11} + Q_{22} - 2Q_{12} + 4Q_{66}\}/8
\end{aligned}
\tag{2}
$$

Figure 4 illustrates the feasible region for laminates *a* and *b* of Table 2, which also share the same bending stiffness. Similarly, Fig. 5 illustrates the feasible region for laminates *d* and *e* of Table 2. However, both Fig. 4 and Fig. 5 reveal that bending isotropy, (ξ_9, ξ_{10}) = (0.00, 0.00), cannot be achieved for any ply angle combinations.

Figures 6 and 7 present lamination parameter points for bending stiffness of a typical Skin panel design, corresponding approximately to (0, ±45, 90°) ply percentages of (44/44/12), or lamination parameter coordinates (ξ_1, ξ_2) = (0.32, 0.16). The points are representative of the designs listed in Table A1 for ply number groupings n = 16 – 19.

For the common angle ply combination leading to extensional isotropy, all three laminate pairings, *a* (*b*), *c* (*f*) and *d* (*e*), in Figs. 4, 3 and 5, respectively, share the same lamination parameter ξ_{10} = 0.0, hence buckling load for the square plate configuration investigated in this article. This arises despite having different lamination parameters, ξ_9 = 0.53, 0.13 and 0.27, respectively. This can be understood from Fig. 6, which illustrates compression buckling contours, superimposed over the lamination parameter design space for standard laminate designs. For aspect ratio a/b = 1.0, i.e. a square plate, the isolines are horizontal, switching to sloping isolines in the mode change region. A constant

lamination parameter ξ_{10} = 0.0 therefore leads to constant buckling load factor across this range of lamination parameters. By contrast Fig. 7 demonstrates sloping isolines for intermediate aspect ratio, a/b = 1.5, and therefore designing for constant buckling factor is less simplistic, since mode changes occur in the centre region of the design space. Because all laminates considered here are fully uncoupled, Figs 6 and 7 are readily developed through a closed form solution.

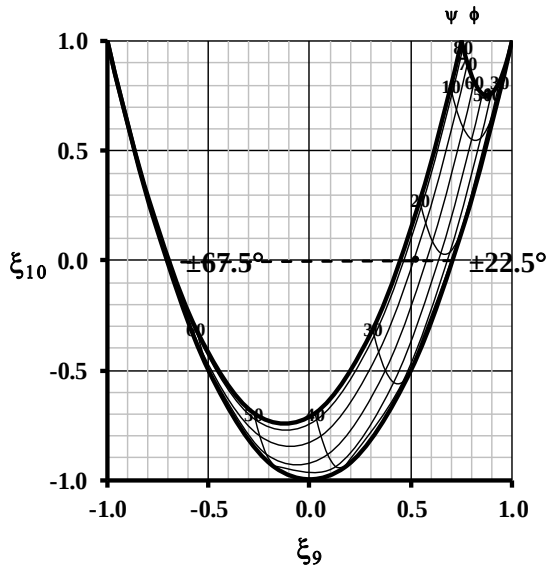

Figure 4: Lamination parameter design space for bending stiffness, representing laminates *a* and *b* of Table 2.

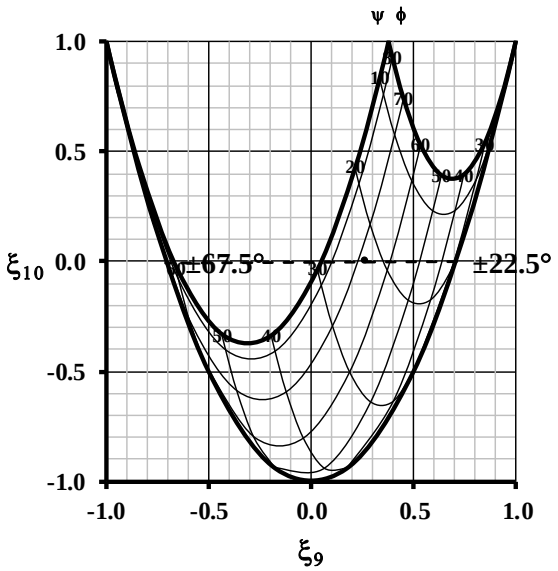

Figure 5: Lamination parameter design space for bending stiffness, representing laminates *d* and *e* of Table 2.

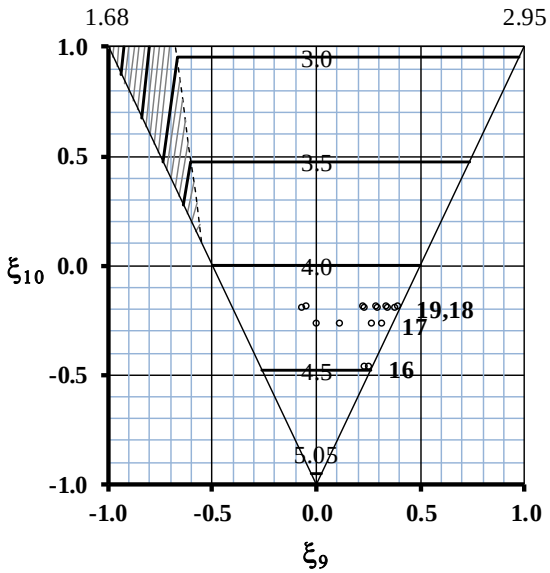

Figure 6: Compression buckling contours for plate aspect ratio (a/b =) 1.0 with lamination parameter points corresponding to designs of Table A1.

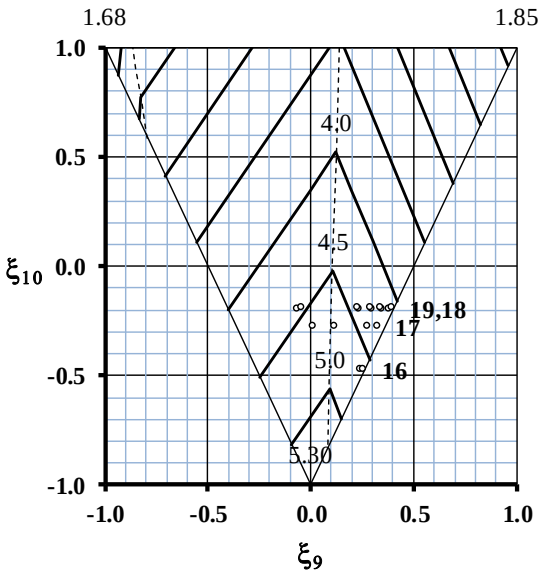

Figure 7: Compression buckling contours for plate aspect ratio (a/b =) 1.5 with lamination parameter points corresponding to designs of Table A1.

3.3 Summary of stiffness matching approach

For the double angle-ply configuration designs, a new design methodology is adopted [3], to match the bending stiffness between standard ply laminates (with 0°, ±45° and 90° fibre directions) and double angle-ply laminates (with ±ϕ° and ±ψ° fibre directions). This is achieved by first establishing a database of designs, based on angle-ply non-crimp fabric architectures, which are now available commercially with bespoke angles. The database contains stacking sequence listing in symbolic form and non-dimensional parameters, to which any fibre angles, thicknesses and material properties can be later assigned.

For balanced angle-ply pairs, the ply angle dependent lamination parameters may be expressed as:

$$\xi_9 = \{(\zeta_{\pm\phi})\cos 2\phi + (\zeta_{\pm\psi})\cos 2\psi\}/\zeta \tag{3}$$

and given $\zeta = \zeta_{\pm\phi} + \zeta_{\pm\psi}$ (= n^3), where ζ is a non-dimensional parameter corresponding to the total contribution to bending stiffness for all n plies in the laminate, the expression becomes:

$$\xi_9 = \{(\zeta_{\pm\phi})\cos 2\phi + (\zeta - \zeta_{\pm\phi})\cos 2\psi\}/\zeta \qquad \xi_{10} = \{(\zeta_{\pm\phi})\cos 4\phi + (\zeta - \zeta_{\pm\phi})\cos 4\psi\}/\zeta \tag{4}$$

or can be simplified further using $\gamma = \zeta_{\pm\phi}/\zeta$, and $\alpha = \cos 2\phi$ and $\beta = \cos 2\psi$, and the double angle relationship $\{\cos 4\phi = 2\cos^2(2\phi) - 1\}$ to give:

$$\xi_9 = (\zeta_{\pm\phi}/\zeta)\alpha + (1 - \zeta_{\pm\phi}/\zeta)\beta \qquad \xi_{10} = (\zeta_{\pm\phi}/\zeta)(2\alpha^2 - 1) + (1 - \zeta_{\pm\phi}/\zeta)(2\beta^2 - 1) \tag{5}$$

From the first of these expressions the relative contributions to bending stiffness of the ±ϕ sub-laminate becomes:

$$\zeta_{\pm\phi}/\zeta = (\xi_9 - \beta)/(\alpha - \beta) \tag{6}$$

which is known *a priori*. Finally, substituting Eqn. (6) into the second expression of Eqn (5) leads to the following quadratic solution for β (= $\cos 2\psi$):

$$\beta = -(\xi_{10} + 1 - 2\alpha^2)/4(\alpha - \xi_9) \pm [((\xi_{10} + 1 - 2\alpha^2)/4(\alpha - \xi_9))^2 - (2\alpha^2\xi_9 - \alpha - \xi_{10}\alpha)/2(\alpha - \xi_9)]^{1/2} \tag{7}$$

The value of α (= $\cos 2\phi$) is solved iteratively until Eqns (6) is balanced, using the target value of β (= $\cos 2\psi$) from Eqn. (7), corresponding to the lamination parameters (ξ_9, ξ_{10}) of the standard ply angle configuration, or indeed to any lamination parameter coordinate of choice. The angle ψ is then solved directly through $\beta = \cos 2\psi$, once the iterative process has converged.

3.4 Post buckling simulation and modelling

Results were generated with the ABAQUS finite element code [7] with a thin plate element (S8R5), using a NAFEMS benchmark 3DNLG-6 for buckling of a quarter flat plate with an initial imperfection when subjected to in-plane shear [8], but modified here to a full plate with compression loading to correctly capture any anisotropic behaviour, as illustrated in Fig. 8.

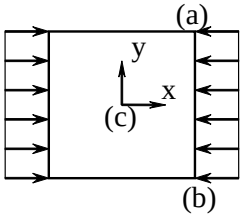

Figure 8 – Compression loaded plate illustrating points (a) – (c) for load-deflection interrogation.

Plate dimensions of 300 mm × 300 mm, together with a range of ply number groupings representing the 12- to 21-ply symmetric laminates of Fig. 1 and Table 1, giving a total thickness H = ($n \times t$ = 12 × 0.15 mm =) 1.8 – 3.15 mm, ensure that the results are representative of the thin plate solution. The material properties were: E_1 = 147 GPa, E_2 = 10.3 GPa, G_{12} = 7 GPa and ν_{12} = 0.27.

Note that equivalent isotropic plate stiffnesses were entered directly into ABAQUS to allow the Eigenvalue buckling load to be verified against the closed form buckling solution. Hence for compatibility, the boundary conditions for all cases were chosen such that at the plate centre, indicated by point (c) on Fig. 8 in-plane displacements, δx and δy, are prevented together with in-plane rotation, i.e. rotation about the z-axis. Out-of-plane displacement constraints, δz, are applied to the plate perimeter. The modified NAFEMS benchmark 3DNLG-6 was found to converge to within approximately 1% of the closed form solution.

4 RESULTS AND DISCUSSION

The effect of stiffness matching, using the double angle-ply designs of Table 2, is revealed in Fig. 9(a) and 9(b) for extensional stiffness and bending stiffness, respectively. Extensional stiffness matching to the 16 ply symmetric design taken from Table A1 produces coincident load paths for all designs up to the bifurcation point. By contrast, bending stiffness matching produces coincident buckling loads ($N_x/N_{x,Iso}$), which are normalized against the equivalent isotropic laminate. The lamination parameters for each set of curves are given in Table 3, where all three designs share the same (ξ_1, ξ_2) for extensional stiffness matching and the same (ξ_9, ξ_{10}) for bending stiffness matching. The angles (ϕ, ψ) required for stiffness matching are also given.

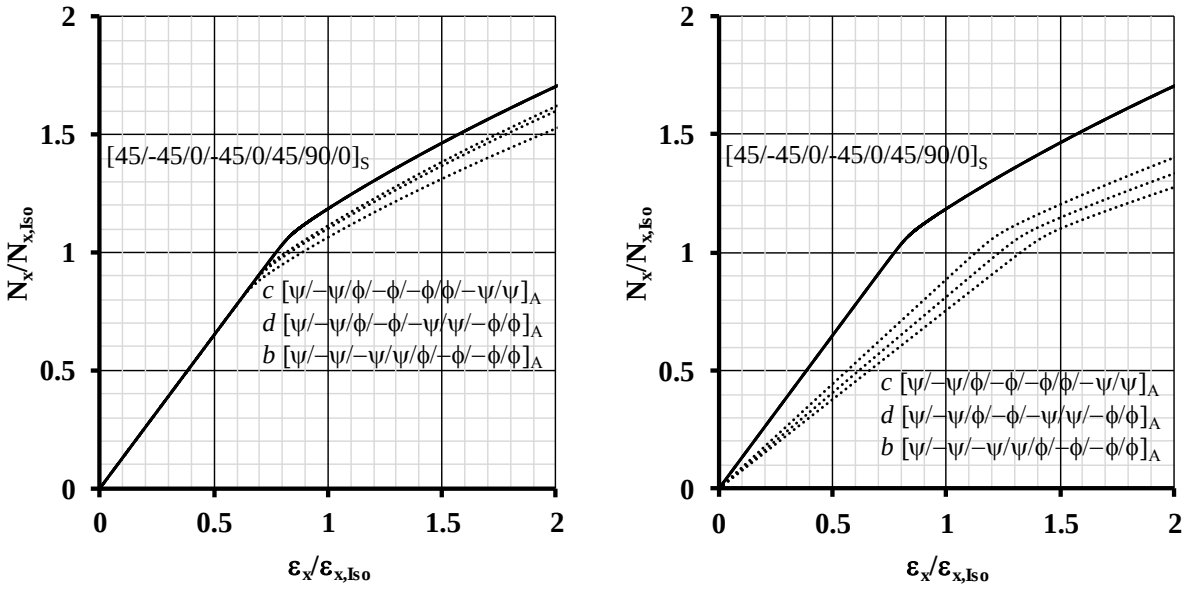

Figure 9: In-plane load-deflection matching for standard (solid line) with: (a) extension stiffness matched and; (b) bending stiffness matched (broken line) double angle-ply laminates, listed in order.

Figure 10 presents a comparison of standard designs from Table A2, which share the same axial stiffness. Here, the equivalent isotropic design, against which the designs are normalised, is also illustrated. Figure 10(a) illustrates a similar pattern to that of Fig. 9(a), in which only the bifurcation points differ, due to a variation in bending stiffness. The gradient of the axial stiffness is essentially unchanged for all the designs, both pre- and post-buckling. The curves nest, i.e., there is no crossing at any point, which confirms that bending stiffness does not influence axial stiffness in the post-buckled state. Load-deflection characteristics, out-of-plane, measured at the centre of the plate, are

un-remarkable since the post buckling response is stable, but do serve to demonstrate the difficulty in determining the bifurcation point. Note that analysis is restricted to compression loading in this study, yet the laminate configurations presented in Fig. 9 are typical of Spar components and therefore subject to shear loading.

	Laminate Ref.:					
	(ξ_1, ξ_2) matched			(ξ_9, ξ_{10}) matched		
Design Parameters	*b*	*c*	*d*	*b*	*c*	*d*
ξ_1		0.25		-0.28	0.15	0.05
ξ_2		0.00		0.12	-0.52	-0.51
ξ_9	0.74	0.37	0.50		0.24	
ξ_{10}	0.50	0.12	0.25		-0.47	
ϕ		57.15°		83.53°	54.22°	58.12°
ψ		12.15°		32.88°	25.99°	28.45°

Table 3: Stiffness matching between laminate 16*a* of Table A1, with laminations parameters (ξ_1, ξ_2) = (0.25, 0) and (ξ_9, ξ_{10}) = (0.24, -0.47), and double angle-ply laminates *b*, *c* and *d* of Table 2.

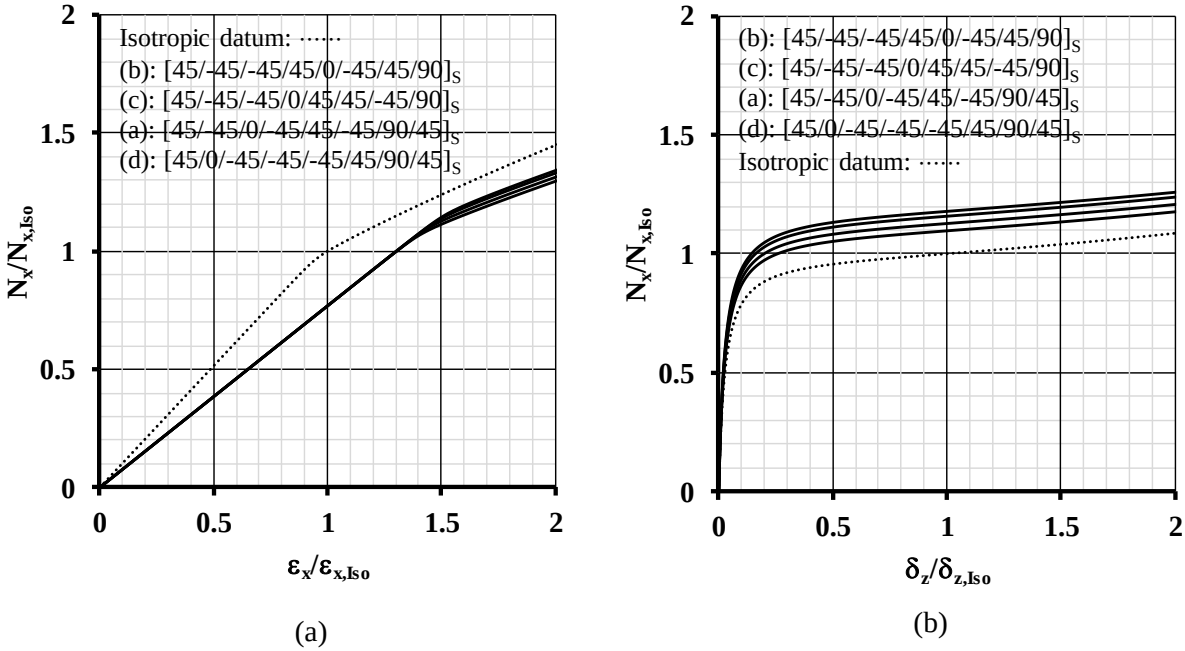

Figure 10: Normalised post-buckling curves for typical Spar designs from Table A2, illustrating: (a) in-plane and; (b) out-of-plane response, with isotropic design shown dotted.

A test was performed to assess whether *Bending-Twisting* coupling, commonly encountered in symmetric designs, produces a variation in the post buckling response. Here, a pseudo quasi-homogeneous coupled laminate with stacking sequence $[45/0/90/45/90/-45/-45/0]_S$ was employed. It possess fully isotropic stiffness properties in both extension and bending, but in addition, possesses *Bending-Twisting* coupling ($D_{16} = D_{26} \neq 0$). The results produce similar load-displacement relationship to the double angle-ply designs in of Fig. 9(a), i.e. the design has the same initial load path, but bifurcation takes place 10% lower than the fully isotropic design.

These observations suggest that the axial stiffness prior to buckling dictates the axial stiffness in the post-buckled state. In all cases, the curves nest, i.e. there is no crossing of the load-deflection paths. This implies that there are no in-plane stiffness improvements in the post-buckled state for symmetric designs, as perhaps might be implied otherwise by observing the load-deflection paths of coupled laminates [9].

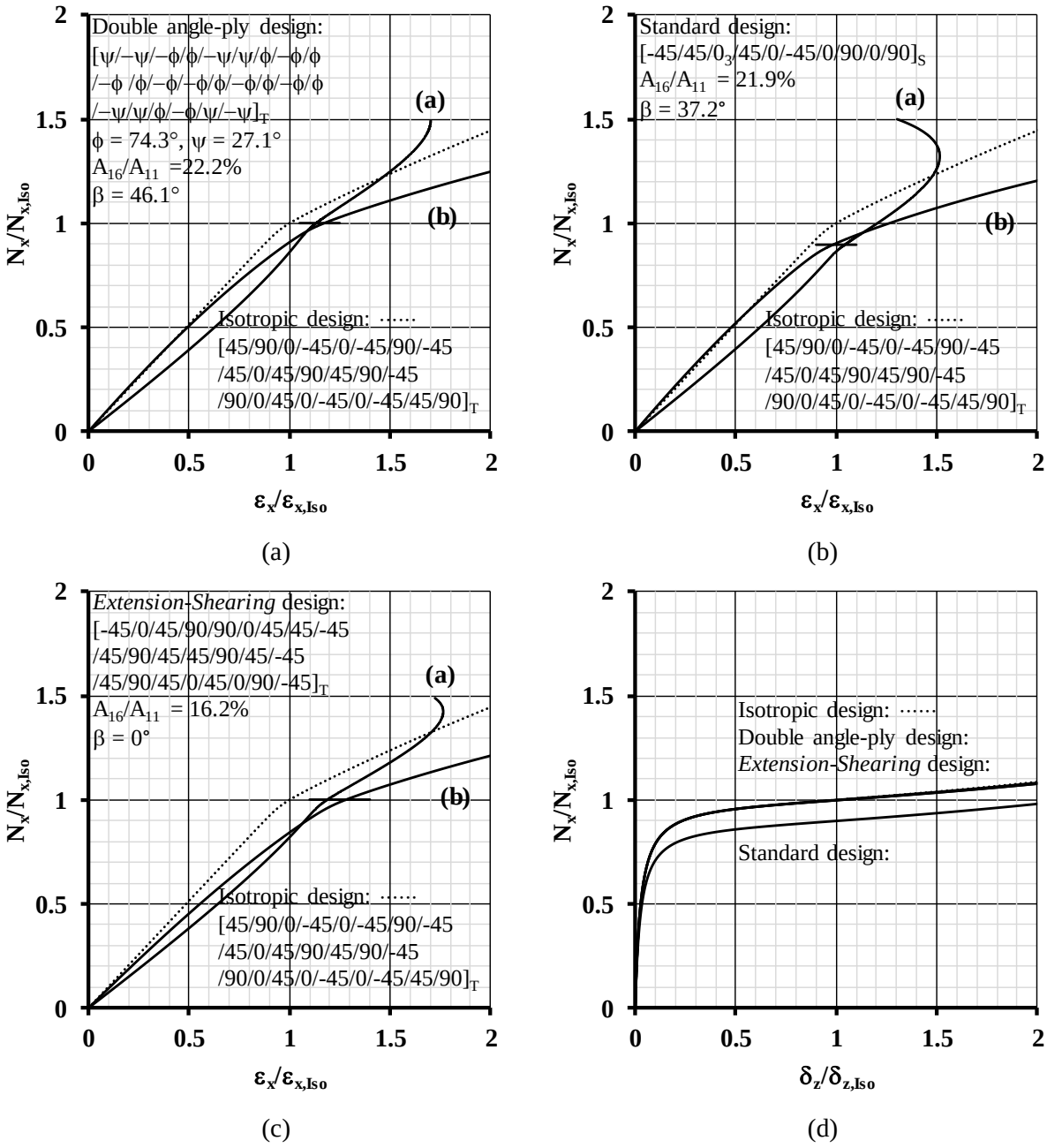

Figure 11: In-plane response of a compression loaded square plate with *Extension-Shearing* coupling for: (a) Double angle-ply design with bending isotropy; (b) Standard design and; (c) Non-standard design, with isotropic design shown dotted. Off-axis alignment, β, to maximise *Extension-Shearing* coupling, A_{16}/A_{11}, is given for each design. Out-of-plane response: (d) for all cases.

Coupled laminates are explored in a final set of results, presented in Fig. 11, using a geometrically non-linear (geometric) analysis within ABAQUS. The designs here possess *Extension-Shearing* coupling behaviour. This form of coupling is achieved through the use of standard ply orientations aligned with and without off-axis alignment. Off-axis alignment is also applied to double angle-ply laminates. However, in order to achieve *Extension-Shearing* coupling, orthotropic designs must be adopted. For this reason, 24-ply laminates are selected for this part of the study, since the solutions of Table 2 have isotropic extensional stiffness properties, which do not change with off-axis orientation. Once again, all designs are compared to an isotropic (datum) laminate, with the stacking sequence given. *Extension-Shearing* coupled skin panels are necessary to introduce bending-twisting coupling

at the wing box level [4]. Each design was therefore selected for maximum laminate level *Extension-Shearing* coupling together with a buckling load matching the fully isotropic design, to demonstrate the feasibility of the proposed passive adaptive wing design.

The off-axis alignment, β, required to maximise *Extension-Shearing* coupling, A_{16}/A_{11}, is given for each of the three designs. Two in-plane load-deflection paths are illustrated in Figs 11(a) – (c), corresponding to opposing corners of the loaded edge of the plate, see Fig. 8. The two corner displacements are not equal due to in-plane anisotropy, or *Extension-Shearing* coupling and therefore the curves split. Fig. 11(d) indicates the out-of-plane response at the centre of the plate is nevertheless unremarkable. However, due to the anisotropic properties of these designs, the in-plane response can appear somewhat unusual and difficult to interpret, and on this occasion, the out-of-plane response of Fig. 11(d) helps to clarify. For instance, the Double angle-ply with off-axis alignment, $\beta = 46.1°$, and *Extension-Shearing* coupled design, which requires no off-axis alignment ($\beta = 0°$), both share identical initial buckling load with the fully isotropic laminate. Whilst the out-of-plane responses of all three laminate designs are coincident, they exhibit very different in-plane behaviour. By contrast, the Standard laminate design, with off-axis alignment, $\beta = 37.2°$, has reduced buckling load since *Bending-Twisting* coupling has also been introduced as a result of the off-axis alignment, which explains the lower curve in Fig. 11(d).

5 CONCLUSIONS

This article has demonstrated the effect of designing for matched stiffness in Bending or Extension, between standard and double angle-ply laminates: Bending stiffness matching allows a range of axial stiffness responses to be realised, all with identical initial buckling load and; Extensional stiffness matching results in identical load paths up the bifurcation point, which differs between the designs presented.

The axial stiffness responses in the pre-buckled state have been shown to be directly linked to those in post-buckled state and no designs were found with improved axial stiffness in the post-buckled state.

A comparison of the responses for competing *Extension-Shearing* coupled designs with identical initial buckling load, revealed similar patterns in the pre- and post-buckled extensional stiffness properties. Competing Standard designs with off-axis orientation, to maximise *Extension-Shearing* coupling, resulted in a significant reduction in the initial buckling strength as a result the unavoidable introduction of *Bending-Twisting* coupling.

REFERENCES

[1] S. Tsai, Keynote: design of composite laminates, *21st International Conference on Composite Materials*, Xi'an, China, 2017.

[2] M. W. D. Nielsen, K. J. Johnson, A. T. Rhead and R. Butler, Laminate design for optimised in-plane performance and ease of manufacture, *Composite structures*, **177**, 2018, pp. 119-128.

[3] C. B. York, New insights into stiffness matching between standard and double angle-ply laminates, *11th Asian-Australian Conference on Composite Materials*, Cairns, Australia, 2018.

[4] C. B. York, Y. B. Murta, and S. F. M. Almeida, A Passive-adaptive Wing for Drag Reduction. *31st Congress of the International Council of the Aeronautical Sciences (ICAS 2018)*, Belo Horizonte, Brazil, 2018.

[5] C. B. York, Characterization of non-symmetric forms of fully orthotropic laminates. *Journal of Aircraft*, **46**, 2009, pp. 1114-1125 (doi:10.2514/1.32938).

[6] C. B. York, On bending-twisting coupled laminates, *Composite Structures*, **160**, 2017, pp. 887-900.

[7] ABAQUS/Standard, Version 6.14. Dassault Systèmes Simulia Corp. 2018.

[8] N.K. Prinja and R. A. Clegg, Assembly benchmark tests for 3D beams and shells exhibiting geometric non-linear behaviour, *NAFEMS, Publication No. R0029*, 1992.

[9] C. G. Diaconu and P. M. Weaver. Post buckling of long unsymmetrically laminated composite plates under axial compression, *Solids and Structures*, **43**, 2006, pp. 6978-6997.

APPENDIX

n	Stacking Sequence	(ξ_1, ξ_2)	(ξ_9, ξ_{10})	Plate Aspect Ratio (*a*/*b*)				
				0.5	1.0	1.5	2.0	2.5
16	*a*: $[45/-45/0/-45/0/45/90/0]_S$	(0.25, 0.00)	(0.24, -0.47)	18.7%	11.5%	6.2%	11.5%	6.4%
	b: $[45/-45/0/-45/0/45/0/90]_S$		(0.26, -0.47)	20.2%		5.1%		5.9%
17	*a*: $[45/-45/90/0/-45/0/0/45/\underline{0}]_S$	(0.29, 0.06)	(0.01, -0.27)	2.6%	6.7%	6.0%	6.7%	6.5%
	b: $[45/-45/0/90/-45/0/0/45/\underline{0}]_S$		(0.12, -0.27)	9.6%		7.9%		4.9%
	c: $[45/-45/0/0/-45/90/0/45/\underline{0}]_S$		(0.27, -0.27)	19.7%		0.9%		1.2%
	d: $[45/-45/0/0/-45/0/90/45/\underline{0}]_S$		(0.32, -0.27)	22.9%		-1.3%		0.0%
18	$[45/0/-45/-45/90/0/0/0/45]_S$	(0.33, 0.11)	(0.23, -0.20)	16.6%	4.8%	1.3%	4.8%	0.4%
	$[45/0/-45/-45/0/90/0/0/45]_S$		(0.30, -0.20)	20.9%		-1.7%		-1.2%
	$[45/0/-45/-45/0/0/90/0/45]_S$		(0.35, -0.20)	24.1%		-3.9%		-2.4%
	$[45/0/-45/-45/0/0/0/90/45]_S$		0.38, -0.20)	26.2%		-5.4%		-3.2%
19	$[45/0/-45/-45/90/0/0/45/0/\underline{0}]_S$	(0.37, 0.16)	(0.23, -0.19)	16.2%	4.7%	1.5%	4.7%	0.5%
	$[45/0/-45/-45/0/90/0/45/0/\underline{0}]_S$		(0.29, -0.19)	20.2%		-1.4%		-1.1%
	$[45/0/-45/-45/0/0/90/45/0/\underline{0}]_S$		(0.34, -0.19)	23.4%		-3.6%		-2.2%
	$[45/0/-45/-45/0/0/0/45/90/\underline{0}]_S$		(0.40, -0.19)	27.1%		-6.1%		-3.6%
	$[45/90/-45/-45/0/0/0/45/0/\underline{0}]_S$		(-0.04, -0.19)	-1.6%		2.6%		3.5%

Table A1: Initial buckling load increases (%) above isotropic datum for symmetric laminates most closely matching typical skin panel properties, (ξ_1, ξ_2) ≈ (0.32, 0.16), for each ply number grouping, *n*.

n	Stacking Sequence	(ξ_9, ξ_{10})	Plate Aspect Ratio (*a*/*b*)				
			0.5	1.0	1.5	2.0	2.5
16	$[45/-45/90/-45/45/-45/0/45]_S$	(-0.16, -0.62)	-6.4%	15.1%	7.8%	15.1%	10.9%
	a: $[45/-45/0/-45/45/-45/90/45]_S$	(0.16, -0.62)	14.9%		12.3%		11.6%
	$[45/-45/-45/90/45/45/-45/0]_S$	(-0.12, -0.76)	-2.4%	18.6%	12.1%	18.6%	15.1%
	$[45/-45/-45/45/90/-45/45/0]_S$	(-0.07, -0.85)	1.3%	20.9%	15.5%	20.9%	18.1%
	b: $[45/-45/-45/45/0/-45/45/90]_S$	(0.07, -0.85)	10.4%		19.7%		19.1%
	c: $[45/-45/-45/0/45/45/-45/90]_S$	(0.12, -0.76)	12.8%	18.6%	17.0%	18.6%	15.9%
	d: $[45/0/-45/-45/-45/45/90/45]_S$	(0.23, -0.48)	18.5%	11.7%	6.5%	11.7%	6.7%
	$[45/90/-45/-45/-45/45/0/45]_S$	(-0.23, -0.48)	-11.9%		2.8%		6.3%

Table A2: ·Initial buckling load increases (%) above isotropic datum for symmetric laminates with (ξ_1, ξ_2) = (0.00, -0.50), which most closely match typical Spar properties, (ξ_1, ξ_2) ≈ (0.00, -0.60).

A second set of non-linear (geometric) analysis results are presented here, using an alternative to the material definition used earlier, where thickness, material properties and orientation were listed for each ply in the stacking sequence within the ABAQUS model. In this alternative approach, the laminate ABD stiffness properties are instead entered directly into the ABAQUS model. However, whilst isotropic and orthotropic results are identical to those presented earlier, the resulting in-plane responses for the coupled designs, presented in Fig. A1, differ significantly from the in-plane behaviour illustrated in Fig. 11. Without experimental validation, it is difficult to know which of the two sets of results are correct.

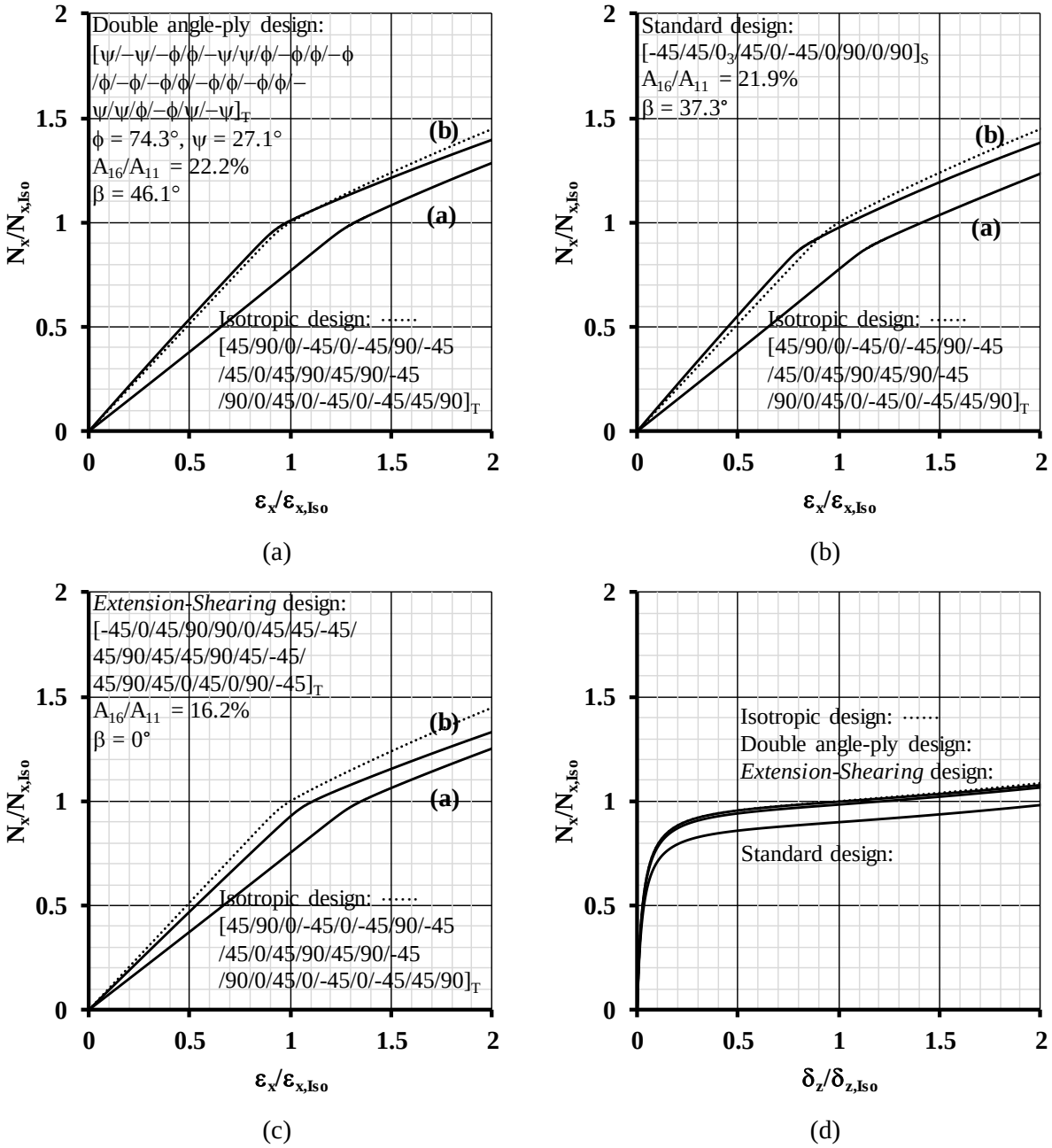

Figure A1: In-plane response of a compression loaded square plate with *Extension-Shearing* coupling for: (a) Double angle-ply design with bending isotropy; (b) Standard design and; (c) Non-standard design, with isotropic design shown dotted. Off-axis alignment, β, to maximise *Extension-Shearing* coupling, A_{16}/A_{11}, is given for each design. Out-of-plane response: (d) for all cases.